YEAST CELL DETECTION AND SEGMENTATION IN BRIGHT FIELD MICROSCOPY

Chong Zhang[1], *Florian Huber*[2], *Michael Knop*[2] *and Fred A. Hamprecht*[3]

[1]CellNetworks, University of Heidelberg, Germany [2]ZMBH University of Heidelberg, Germany [3]HCI/IWR Heidelberg, Germany

ABSTRACT

We present a method for detecting and segmenting yeast cells in bright field microscopy images from which cells are often almost transparent. A classifier is firstly trained to detect edges of cells of interest. A label cost model with cardinality constraints then simultaneously detects cell centers and clusters cell edge points, using Integer Linear Programming. For a noisy or partial edge clustering, an additional step of contour fitting or seeded watershed is applied for segmentation. Results demonstrate that our method can consistently detect and segment yeast cells from a variety of datasets, and its performance is close to that of manual segmentation.

Index Terms— bright field microscopy, cell detection, segmentation

1. INTRODUCTION

The purpose of this study is to find a generic and robust way of segmenting yeast cells for a high-throughput imaging study. Bright field microscopy is the simplest optical microscopy technique but is the best to assess morphology, health, and focus of cells. Analysis of cells based on bright field rather than fluorescence microscopy images is attractive for biological reasons, but rises hard segmentation problems: Cells in these images are almost only distinguishable by their outer membrane. Displacements of cells relative to the focus plane result in missing boundaries and varying contrast patterns. Cells are often densely packed and may overlap with each other. They are also often imaged with uneven illumination and may be contaminated by other particles or dirt. In summary, challenging issues include broken boundaries, poor contrast, partial or changing halo, overlap with out-of-focus cells, and imaging artifacts. Fig. 1 shows examples from a variety of datasets. This problem has attracted much attention in the past decade [**?**, 1, 2, 3, 4], with proposed solutions ranging from intensity based thresholds to graphical models, watershed transform, active contours, circular Hough transform, etc. Some publicly available software packages also include methods to address this [6, 7, 8]. However, as also commented in [5], most of these methods and tools work on "clean" images such as those with clear, consistent boundary patterns and well separated cells. For example, the approach in [9] detects cell centers first and then uses a polar plot to find the best cell contours. But this method works on images that exhibit a relatively low degree of cell crowding and density, and it also relies on a consistent diffraction fringe pattern to locate cell contours. Additionally, some need images taken slightly out of focus [7] or combined use with fluorescent images. To deal with a general scenario as aforementioned, a good algorithm should allow segmenting images with either dense or sparse cells. It should also generalize well such that a generic parameter setting can be used for similar images. Furthermore, it should be able to detect "good" cells useful for further biological measurements (e.g. whole cell morphology and size) and discard "bad" ones, e.g. the out-of-focus ones. Our approach satisfies these criteria. It augments a label cost model (e.g. [10]) with cardinality constraints to simultaneously detect good cell centers using a Hough transform and cluster cell edge points obtained from an edge classifier. The model is optimized using Integer Linear Programming (ILP). Subsequently, individual cells are described either by a smooth closed curve fit to the clustered edge points or a watershed based segmentation. We build on ideas from [11] (which however does not cluster edge points) and [12] (which however does not allow for label costs). An illustration of the framework is shown in Fig. 2.

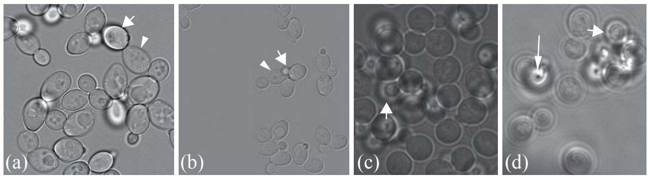

Fig. 1: Dataset 1-4 (a-d) examples. In-focus cells (*arrow heads*) are overlap with out-of-focus ones (*arrows*) in images with low contrast (b), uneven illumination (d), other particles or dirts contamination (*long arrow*), and artifacts (c, d).

2. METHOD

2.1. Detecting edge candidates

To ensure detecting "good" yeast cell boundaries in bright field microscropy with varying patterns, a trainable classifier seems to be the right choice. We choose to train a pixel based

The authors thank Daniel Kirrmaier for acquiring bright field images.

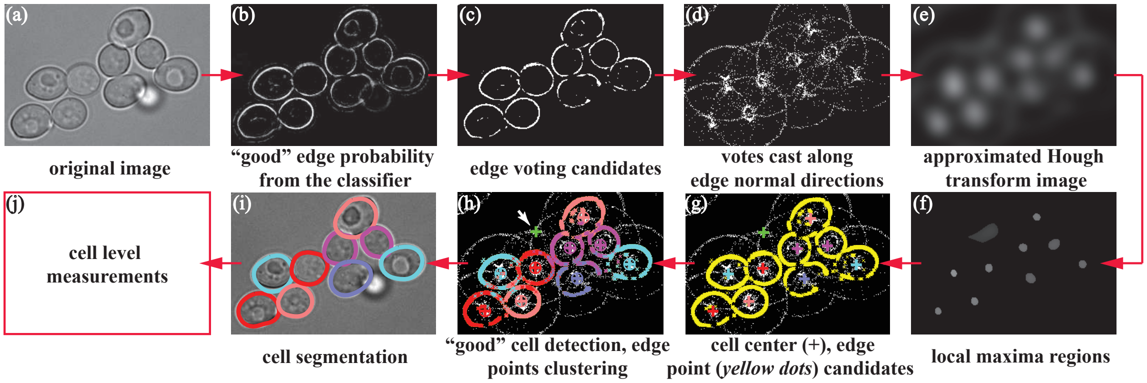
(a)
original image
(b)
"good" edge probability from the classifier
(c)
edge voting candidates
(d)
votes cast along edge normal directions
(e)
approximated Hough transform image
(f)
local maxima regions
(g)
cell center (+), edge point (*yellow dots*) candidates
(h)
"good" cell detection, edge points clustering
(i)
cell segmentation
(j)
cell level measurements

Fig. 2: Illustration of the cell detection and segmentation procedure. The original image (a) is first applied with a good cell edge classifier and the prediction (b) is binarized (c) to determine edge voting candidates. After a Hough transform (d, e) to determine cell center candidates (f, g), a label cost model is built and optimized (h) to both discard false cell centers (*white arrow*) and cluster edge points belonging to the same cell (*color labeled edge points*). Finally individual cells are segmented (i), either by fitting a closed spline curve each cell contour or a seeded watershed method, for further measurements (j).

classifier, ilastik [13], to discriminate: (1) boundaries of in-focus cells; (2) in-focus cells; (3) out-of-focus cells; and (4) background. The posterior probabilities for class (1) are binarized and assumed to be the edge point candidates domain. A subset may be used, compromising computational effeciency and sufficient edge candidates. Sampling rate may vary according to the size of object of interest in the images.

2.2. Detecting cell center candidates

Cell center candidates are detected through a Hough transform by casting votes from the edge point candidates. For each candidate, votes are discretely cast and counted along a single voting line segment on the edge normal direction (e.g. approximated by image gradient direction). The line segment has a length of $2l$ (in pixels), similar to cell size in images, and centered at the edge point. This discrete voting scheme gives discontinuous vote distribution in the Hough transform image, thus a Gaussian lowpass filter is applied to approximate the continuous voting, with filter size l and standard deviation $\frac{1}{6}l$. In order to avoid unnecessary computation, some preprocessing can be performed to eliminate the most obvious wrong candidates, such as a H-maxima transform to suppress maximas with too low height, or a size filter to eliminate too small and too large local vote regions. Similarly, an edge point candidate can be discarded if it is too far from all the center candidates (e.g. distance larger than $2l$). Note that all parameters are specified as constant multiples of the approximate cell diameter $2l$, which can be either specified by the user or inferred from the imaging settings of each dataset.

2.3. Label cost model: selecting cell centers, clustering edge points

Each local maximum corresponds to a hypothesis about the presence of a cell approximately centered at this particular location. Typically, a greedy non-maxima suppression is applied to first find the true cell centers, subsequently each edge point is assigned to its highest voted center or even to its closest voted center using e.g. k-nearest neighbors method. Instead, a label cost model is introduced, which simultaneously optimizes the labels of all edge points, i.e. which cell center an edge is assigned to as well as the set of "active" cell centers while maintaining cardinality. By doing so, it offers a global optimal taking into account both the cost for assigning an edge to a cell center candidate and the estimated probability that a cell center candidate is a true positive. The penalty for assigning the ith edge element $(i{\in}1,\ldots,N)$ to the jth cell center candidate $(j{\in}1,\ldots,M)$ is given by the shortest Euclidean distance from its L_i sampled votes to the center: $s_{ij}{=}\min\{d_{jk_i}\}, k_i{\in}1,\ldots,L_i$. We set $L_i{=}2$, i.e. only two end points of the cast line. To allow discarding false center candidates, each center candidate is given a unary potential that measures how well it is surrounded and thus supported by edge points. A cell candidate j with larger value ρ_j is preferred to be an active cell center, e.g. ρ takes the votes density.

This model is formulated as an ILP to find the subset of local maxima corresponding to true cells. Let $\{a_j\}$ be the binary indicator variables associated with the M maxima that persist after the filtering steps. A variable is set to 1 if the hypothesis actually corresponds to an active cell, or to 0 otherwise. Similarly, binary indicator variables$\{c_{ij}\}_{N\times M}$ takes 1 when edge element i belongs to cell j and 0 otherwise.

Three constraints are introduced to specify the relationship between an active cell center and the edge points assigned to it. First, each edge element is assigned to exactly one cell: $\sum_{j=1}^{M} c_{ij}{=}1$. Second, an edge element can only be assigned to a center point that is active. To avoid treating inactive points as a special case, the constraint can be expressed as $c_{ij}{\leq}a_j, \forall i$ or equivalently $\sum_{i=1}^{N} c_{ij}{\leq}Na_j$. Finally, the cardinality constraint specifies that each cluster has a lower limit ℓ

Table 1: Experimental settings for datasets 1-4 (from *top* to *bottom*).

Strain background	Mean cell area	Microscope	Camera	Magnification	NA	Pixel size	Artifacts
Diploid yeast	18 μm^2	DeltaVision	CoolSnap HQ2	60x	1.42	107 nm	-
Diploid yeast	18 μm^2	DeltaVision	EDGE	60x	1.42	215 nm	-
Haploid yeast	10 μm^2	Nikon Eclipse Ti	Andor Neo	150x	1.40	43 nm	ring like
Haploid yeast	10 μm^2	Nikon Eclipse Ti	Andor Neo	100x	1.40	43 nm	ring like

on the number of voting elements it must contain. Altogether, our model results in the following optimization problem:

$$\begin{aligned}\min_{\{c_{ij}\},\{a_j\}} & \sum_{i=1}^{N}\sum_{j=1}^{M} c_{ij}s_{ij} + w\sum_{j=1}^{M}\frac{a_j}{\rho_j},\\ \text{s.t.}\quad & a_j \in \{0,1\}, \forall i \in 1,\ldots,N\\ & c_{ij} \in \{0,1\}, \forall i \in 1,\ldots,N, \forall j \in 1,\ldots,M\\ & \sum_{j=1}^{M} c_{ij} = 1, \forall i \in \{1,\ldots,N\},\\ & \sum_{i=1}^{N} c_{ij} \le N a_j, \forall j \in \{1,\ldots,M\},\\ & \sum_{i=1}^{N} c_{ij} \ge \ell a_j, \forall j \in \{1,\ldots,M\},\end{aligned}$$

where w is a constant to balance the penalties associated with activating cell centers and assigning edge candidates. In this study, $w \in [0.05, 0.2]$ was a good choice.

The objective function was minimized using Gurobi [14]. The optimization process can be sped up by making the clustering matrix $\{c_{ij}\}$ sparse using a spatial proximity criterion. Instead of optimizing the whole image at once, which contains thousands of edge points and hundreds of center points, splitting small blocks of subimages with certain overlap on the boundaries can also be considered.This is similar to making the clustering matrix sparse.

2.4. Segmentation

The optimized binary indicator variables $\{c_{ij}\}$ specify which active cell center an edge point is assigned to. Ideally, those sharing the same cell label delineate this cell's contour. However, the resultant clustered edge points can be noisy and often reveal only partial cell boundaries. Thus, an additional contour post-processing or segmentation step is mostly desirable.

We evaluated two options: 1) A smooth spline (with a periodic boundary condition) fit to a sparse subset of the edge points, using a least squares method. Additionally, noisy clustered edge points can be pre-filtered by setting a range for the radius, i.e. the distance between the cell center and the edge point. For example, wrongly clustered edge points, such as those belonging to other cells or to the nuclear membrane inside the cell can be discarded. In our case, the range was set to $[0.3l, 1.1l]$. 2) A seeded watershed segmentation. Only the detected cell centers were used as the seeds, while the information from clustered edge points were not used. Standard procedure would apply seeded watershed directly on the original images, but this did not work for bright field images. Instead, it was applied to the distance transform map calculated on the combined edge and background probability maps from the trained classifier.

3. EXPERIMENTS AND RESULTS

In order to evaluate the generality and robustness of our approach, we tested it on four datasets (47 images in total) that differ in sample preparation and imaging equipment and conditions, such as strain background, instrumentation settings, artifacts, etc. Therefore, the resultant bright field images exhibit yeast cells with distinctive appearances (see Fig. 1). The detailed experimental settings are listed in Table 1. Visual inspection of the results can be found in Fig. 3. In general, contour curve fitting provided smoother cell delineation and was able to segment more cells. And watershed usually gave more noisy cell contours, which is often not biologically meaningful in terms of cell morphology. Note that although segmented cells all appear red, each cell is fit independently thus having a distinct identity.

The area overlap was used as the quantitative accuracy measure M_{AO}. It is calculated based on the computer segmented (CS) region R_{CS} and the manually segmented (MS) region R_{MS}: $M_{AO}{=}(R_{CS}{\cup}R_{MS})/(R_{CS}{\cap}R_{MS}){\times}100$. Due to the high cell density, we randomly selected $10{-}20\%$ of cells from each image and manually segmented them to provide the ground truth. Cells with missing contours (e.g. overlapping with out-of-focus cells) were not considered, in order to avoid ground truth uncertainty. In this subset, M_{AO} was calculated on the cells that were also segmented by the computer. Results are summarized in Fig. 4, including a comparison with those obtained using CellX [5], which is dedicated to dealing with crowded cells and various types of microscopy data. In the top plot, similar M_{AO} values were obtained, except for dataset 2 and 4 when using CellX. This is probably due to the less image contrast and smaller cell size in image. However when looking at the lower plot, watershed failed to segment a large number of cells. This is much more noticeable in more challenging datasets like 3 and 4. This suggests that it is helpful to make use of clustered edge points from our model. CellX was not able to segment most of the cells, especially for dataset 2. This is probably because these images have small cell size in image, or with strongly varying cell boundary patterns and low contrasts.

Finally, the M_{AO} of the manual segmentation from a different expert than the one who provided the ground truth were

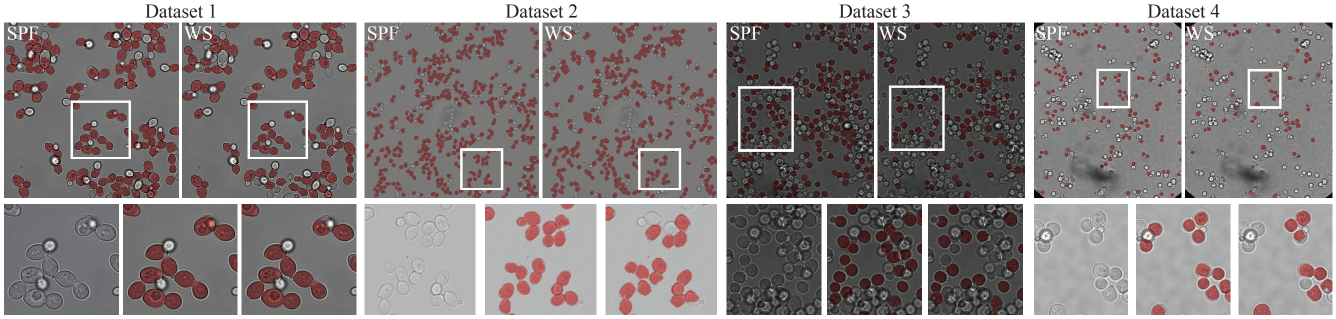

Fig. 3: Example results from the four datasets. (*top*) Segmentation (*red* with transparency) overlaid on original images using spline fitting (SPF) and watershed (WS) based methods. (*bottom*) Zoom-in views of: original image, SPF, and WS images.

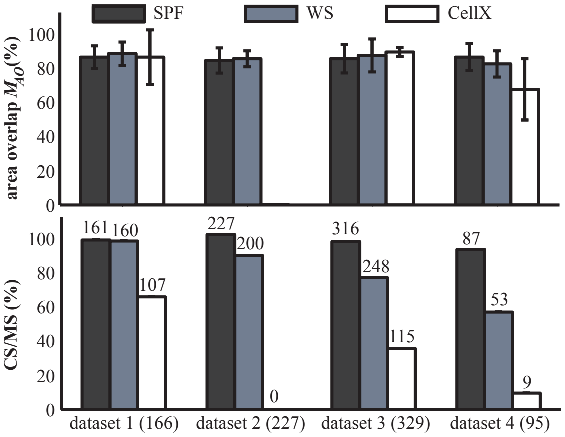

Fig. 4: Quantitative evaluation in datasets 1-4.

calculated. On average, the area overlap ratio is slightly over 90%, resulting in 5-7% higher than those of the computer segmentation in Fig. 4. This not only suggests that our method can almost compete with manual segmentation, but also that identifying individual cell regions is very challenging due to the relatively large inter-variability among human labels.

4. DISCUSSION

This paper presents an approach to extract cells from images with low contrast and with densely crowded cells. Our method is both robust across diverse imaging conditions and able to discriminate out-of-focus cells. Most of the parameter settings are associated with one parameter, comparable to mean cell size in pixels, thus easy to determine and use. This single parameter proved capable of handling most yeast cells in the images, except exceptionally large or small dividing cells. But if these cells are of interest, then probably another step with different value should be performed. The fact that an initial edge classifier is used makes our approach robust to large varieties of yeast cells in bright field microscopy. Since there was no explicit assumptions of special characteristics from bright field images, we expect that the method is general and should be applicable to other modalities such as phase contrast microscopy, and also to other type of cells with different convex shapes.

5. REFERENCES

[1] S.C. Chen, *et al.*, "A Novel Graphical Model Approach to Segmenting Cell Images," in *IEEE CIBCB*, 2006.

[2] M. de Carvalho, *et al.*, "Morphological segmentation of yeast by image analysis," *Image Vision Comput*, vol. 25, no. 1, pp. 34–39, 2007.

[3] R. La Brocca, *et al.*, "Segmentation , tracking and lineage analysis of yeast cells in bright field microscopy images Timelapse microscopy," in *1st Int Workshop on Pattern Recognition in Proteomics, Structural Biology and Bioinformatics*, 2011.

[4] M. Tscherepanow, *et al.*, "Automatic Segmentation of Unstained Living Cells in Bright-Field Microscope Images," in *Int Conf on Mass Data Analysis of Images and Signals*, 2008, pp. 158–172.

[5] C. Mayer, *et al.*, "Using CellX to Quantify Intracellular Events," *Curr Protoc Mol Biol*, no. 101, 14.22, 2013.

[6] A.E. Carpenter, *et al.*, "CellProfiler: image analysis software for identifying and quantifying cell phenotypes," *Genome Biol*, vol. 10, no. 7, R100, 2006.

[7] A. Gordon, *et al.*, "Single-cell quantification of molecules and rates using open-source microscope-based cytometry," *Nat Methods*, no. 4, pp. 175–181, 2007.

[8] "Celltracer," `http://www.stat.duke.edu/research/software/west/celltracer/`.

[9] M. Kvarnström, *et al.*, "Image analysis algorithms for cell contour recognition in budding yeast," *Opt Express*, vol. 16, no. 17, pp. 1035–1042, 2008.

[10] A. Delong, *et al.*, "Fast Approximate Energy Minimization with Label Costs," in *CVPR 2010*.

[11] O. Barinova, *et al.*, "On detection of multiple object instances using Hough transforms," *IEEE T Pattern Anal*, vol. 34, no. 9, pp. 1773–1784, 2012.

[12] B.J. Frey, *et al.*, "Clustering by Passing Messages Between Data Points," *Science*, vol. 315, no. 5814, pp. 972–976, 2007.

[13] C. Sommer, *et al.*, "ilastik: Interactive learning and segmentation toolkit," in *ISBI 2011*.

[14] "Gurobi optimizer," `http://www.gurobi.com/`.